RESEARCH ARTICLE

A Flavonoid-rich Fraction of *Alternanthera pungens* Ameliorates Hyperglycaemia -mediated Memory Dysfunction in Diabetic Rats

Sayyada S Momina[1], Kumaraswamy Gandla[2*]

[1]*Department of Pharmacognosy and Phytochemistry, Chaitanya (Deemed to be university), Gandipet, Himayathnagar (Vill), Hyderabad, Telangana, India.*
[2]*Department of Pharmacy, Chaitanya (Deemed to be university), Gandipet, Himayathnagar (Vill), Hyderabad, Telangana, India.*

Received: 02nd September, 2023; Revised: 22th October, 2023; Accepted: 16th November, 2023; Available Online: 25th December, 2023

ABSTRACT

The central nervous system (CNS) undergoes alterations due to persistent hyperglycemia and cholinergic dysfunction, leading to cognitive impairment associated with diabetes (T2DM). Animal studies have shown that acetylcholinesterase (AChE) inhibitors and anti-diabetics are effective. Considering the impressive potential of natural products in treating DM and AD, the present research set out to assess the neuroprotective effects of a methanolic extract of *Alternanthera pungens* (MEAP) against cognitive impairment in mice caused by hyperglycemia. Hence, we used the mobile workforce management (MWM) and enterprise performance management (EPM) assays to analyze for cognitive impairment in diabetic rats. 30 days after the initiation of T2DM, rats had hyperlipidemia, increased escape latency in EPM tasks, and decreased time spent in the TSTQ during probe trials in the MWM. They also displayed notable and persistent hyperglycemia throughout training trials. Changes in blood glucose, lipid, and liver profiles, as well as performance in MWM and EPM tests, were averted in STZ-induced T2DM rats treated with MEAP (200 and 400 mg/kg). In a separate series of experiments, flavonoids (i.e., quercetin and rutin) were detected by the standardization of the extract using high performance thin layer chromatography (HPTLC). Inhibitory actions against alpha-amylase and alpha-glucosidase demonstrate that both of these flavonoids are potent antidiabetic agents that reduce intestinal glucose absorption. Lastly, the inclusion of these flavonoids in the extract from *A. pungens* is responsible for its action, suggesting that it may provide a novel strategy for preventing cognitive deterioration in diabetes.

Keywords: Diabetes, Alzheimer's disease, *Alternanthera pungens*, Cognitive impairment, Standardization, High performance thin layer chromatography, Rutin, Quercetin.

International Journal of Pharmaceutical Quality Assurance (2023); DOI: 10.25258/ijpqa.14.4.41

How to cite this article: Momina SS, Gandla K. A Flavonoid-rich Fraction of *Alternanthera pungens* Ameliorates Hyperglycaemia -mediated Memory Dysfunction in Diabetic Rats. International Journal of Pharmaceutical Quality Assurance. 2023;14(4):1075-1089.

Source of support: Nil.

Conflict of interest: None

INTRODUCTION

People throughout the globe are dealing with the devastating effects of diabetes, a chronic illness that affects not only their lives but also their families and communities. Although T1DM and T2DM are more well-known nowadays, a newer variant of the disease called type 3 diabetes mellitus (T3DM) has just recently been discovered.[1] This less common kind, which shows up as insulin resistance (IR) in the brain, might have a huge influence on neurocognition and add to the causes of AD.

Amyloidosis is a condition that impacts several tissues and is caused by the buildup of fibrillary proteins. The disorder is identified by the presence of amyloid deposits, and the symptoms might vary depending on the afflicted area. There is emerging evidence linking insulin resistance to the onset of AD.[2-5] IDE controls intracellular domain levels of insulin, amyloid precursor protein (APP), and Aβ protein in living organisms, as stated by Farris *et al*.[6] This research revealed that hyperinsulinemia, glucose intolerance, and cerebral insulin resistance were present in T2DM-rats caused by a mutant IDE. The newly acknowledged relationship among hyperinsulinemia, diabetes, and neurodegeneration or neuronal death may be mediated by IDE hypofunction, which suggests that IDE hypofunction may be the basis or a contributor to some types of type 3 and type 2 diabetes.[7] Hence, in healthy individuals, IDE decreases Aβ, controls insulin levels, and breaks down the APP intracellular domain (AICD).[8] Therefore, insulin, IDE, and Aβ were all involved in a regulating interaction. The accumulation of Aβ within neurons leads to neurodegeneration or neuronal death, which is a symptom of T3DM or brain IR, since insulin may not have been able

**Author for Correspondence: drkumaraswamygandla@gmail.com*

to drive its clearance in this scenario.[9,10] Whether aberrant Aβ expression and protein processing cause or are a result of T3DM and brain insulin resistance is a matter of contention. Regarding the idea of type 3 diabetes being a consequence, IR in the brain may be caused by Aβ poisoning.[11]

Important risk factors for type 2 diabetes include an insulin resistance condition, which may impair neuronal functioning and cognitive abilities when combined with an abnormally high insulin level and a relatively low insulin activity in the periphery.[12,13] As a result, memory problems may be strongly associated with cognitive decline, decreased cerebrocortical glucose metabolism, shrinkage of the hippocampus, and the formation of neuritic plaques.[14,15]

T3DM emerges when insulin-sensitive nerve cells lose sensitivity to the hormone, which is necessary for daily functioning, including learning and cognition.[16-18] Several studies have linked insulin shortage to AD along with its linked cognitive loss.

In this work, we examined how hyperglycemia affected behavioral measures in a diabetic mouse model.

MATERIALS AND METHODS

Collection of Plant Materials

Leaf samples of *Alternanthera pungens* were gathered from the campus of Osmania University in Hyderabad, Telangana, India. Plant No. 13/Hort/MADP/2011-12 (Authentication No. 1) was identified and certified by Dr. A. Vijaya Bhasker Reddy, Professor at Osmania University's Division of Botany in Hyderabad, Telangana, India. For future tests, 1.2 kg of fresh *A. pungens* plant components were meticulously gathered.

Preparation of Extract

The 1.2 kg fresh entire plant of *A. pungens* was washed and blot-dried under running water. After being cleaned of its roots, the plant material was dried in the shade for a further two weeks before being ground into a powder and weighed at 80 gm. We employed the maceration technique to sequentially extract the plant components using solvents. We used methanol to extract 80 gm of shade-dried powder by macerating it in 250 mL of solvent for a week while stirring it occasionally. The samples were filtered using Whatman filter-1 and the methanol extract produced after triple maceration was pooled until the crude powder was exhausted. The powdered drug was air-dried and then fractionated further. Excess solvent was removed from the combination by evaporating it at 37°C under decreased pressure (-760 mmHg) using a rotary evaporator (HEIDOLPH, Germany), resulting in a sticky substance that was then placed in a desiccator until additional phytochemical screening could be performed.[5]

Preliminary Qualitative Phytochemical Analysis

Analysis of phytochemicals was carried out following previously published methods. The following substances were assessed using qualitative methods: glycosides, alkaloids, proteins, saponins, lipids, and phytosterols/terpenes.

Chemical Characterization of the Plant Extract

Column chromatography

Over a silica gel column (60–120 mesh), 10 g of extract was chromatographed with solvents of varying polarities. An array of silica gel columns was loaded with the mixture (Merck, India), and the elution process began with pet ether before progressing through eluents containing progressively higher concentrations of ethyl acetate (in 90:10, 80:20, 70:30, and 50:50). TLC was performed on all of the samples that were obtained. Some fractions had their Rf values merged with others based on their TLC profiles.[19]

Thin layer chromatography

Different solvent solutions, including 9.5:0.5 toluene, 9:1 ethyl acetate, 7:3 chloroform, and 1:1 methanol, were tested in a Thin layer chromatography (TLC) developing setup with a twin-through chamber. Metal plates were used for the fraction runs. Changing the solvent ratios used to create the solvent system helped find the best solvent for identifying the chemical. The plate was stained with polymolibdic acid (PMA) stain reagent, and the spot was visualized by heating it until the desired color appeared. The formula for determining the retardation factor (Rf) was used.[20]

IR and NMR analysis

Spectra were taken using a Bruker Alpha TKBR and ATR spectrophotometer to record infrared light. To obtain ^{1}H and ^{13}C-NMR spectra, TMS was used as an IS in a Bruker AV NMR equipment with 5 mm 1H and 13C magnets running at 500 MHZ.

LC-MS-MS identification

The fractions were analyzed using an Agilent Model: 6540ba Qtof - Infinity 1290 QTof LC-MS (Agilent, India) fitted with an ESI. These are the detection settings that worked best: To determine the identity of a drug that was isolated, chromatographic conditions were established. The whole wavelength range was scanned, from 190 to 400 nm. Conditions for mass spectrometry included a negative ion mode, 40 psi of atomization gas pressure, 9 l/min of dry gas velocity, 350°C of drying temperature, 3,000 volts of ionization voltage, electrospray ionization (ESI), auto MSn for anion detection, and a scanning range of 200 to 800 m/z.

Standardisation by HPTLC technique [21]

To identify quercetin in dried *A. pungens*, a sensitive and dependable high-performance thin layer chromatographic technique has been devised. Chromatography was used to separate the *A. pungens* chloroform extract on silica gel 60 F254 plates. The mobile phase entailed ethyl acetate and pet ether (3:7).

Quercetin and rutin standard stocks, as well as the crude methanol extract (M1) and chloroform fraction (C1), were produced in methanol at 3 mg/mL. To get concentrations varying between 10 to 140 µg/mL, the standard stocks were further diluted. To achieve the desired linearity (100–1400 ng/band), each of the dilutions (10 µL) was loaded onto the HPTLC

column using a microliter syringe that was attached to the applicator. We followed the rules set forth by the International Conference on Harmonization (ICH) while conducting the validation.

For each biomarker, repeat analysis was used to assess the accuracy of the suggested HPTLC techniques. After adding 50, 100, and 150% of 200 ng of each biomarker – Quercetin and Rutin – to the standards, we determined the recovery percentage. To determine the dependability of the method under typical conditions, we tested the suggested HPTLC methods' robustness by seeing how they fared when exposed to small, intentional changes to the make-up of the mobile phase, the amount filled to saturation, and the time taken for saturation. For the HPTLC analysis, the mobile phases were made using ethyl acetate and pet ether (3:7). In the study, the period of saturation also ranged up to 30 minutes.

Selection of suitable solvent

To choose the optimal solvent, we tested them for their inhibitory actions on alpha-amylase and glucosidase *in-vitro*.

Our decision to test the methanolic *A. pungens* extract for its anti-diabetic properties was based on the fact that it contained more phytoconstituents than the other three extracts (pet ether, chloroform, and hydroalcoholic). Additionally, the *in-vitro* anti-diabetic activity suggested that the methanolic extract had the best anti-diabetic potential.

Acute toxicity study

According to OECD standards 423, acute oral toxicity experiments using methanolic extract of *A. pungens* (MEAP) showed that it was fit for consumption. The administration of 2000 mg/kg MEAP to animals resulted in no drowsiness, toxicity, or abnormal behavior. More than 2,000 mg/kg was determined to be the LD50 for MEAP (OECD, 2001). The ED50 of MEAP was found to be 200 and 400 mg/kg, and these dosages were chosen for the experiment since the ED50 is often characterized as being 10% of the LD50.

Animals

Wistar rats were utilized, and each was weighed. They were kept in typical conditions for 28 days, with a regular diet of rat pellets and water availability at all times. The animal experiments were done as per norms and regulations in compliance with the instructions of CPCSEA with registration number CPCSEA/IAEC/JLS/16/07/21/51. Rats were housed in groups of three, with availability of water and food, at 25 ± 1°C and a RH of 60 ± 10% under continual observation. All of our behavioral assessments took place between 10 a.m. and 4 p.m.

Animal grouping

Five of each animal was placed in each of the groups (Table 1).

Evaluation of antidiabetic activity

- *OGTT*[22]

The OGTT of rats that had fasted overnight in controlled environments was done by pricking their tails. After checking fasting blood glucose levels, researchers gave subjects 2 g of glucose per kg of body weight. After that, the animals' BGLs were noted at 30, 60, and 120 minutes. We used a formula to determine each group's area under the curve (AUC).

Evaluation of lipid profile

Cholesterol, HDL cholesterol, and triglycerides were estimated using the protocol laid forth for enzymatic kits.

Evaluation of liver parameters

The estimate of SGOT and SGPT followed the protocol outlined for enzymatic kits.

Evaluation of behavioral activity

- *Morris water maze*

It entails a circular water pool.[23] Mice were taught to use visual clues in their surroundings to find a hidden platform under the water's surface and use it to escape the labyrinth. The MWM features a tank with a diameter of 140 centimeters that maintains water at a temperature of 282°F. A deck was set up in the center of the pool, which had been sectioned off into quarters (Q1, Q2, Q3, and Q4). The MWM was housed in a spacious room with several colored markers strategically placed around the room's perimeter. Over the four days of training, four different baselines were employed for each mouse. The "Escape latency" is the duration to discover the secret landing platform. After the platform was taken away from the mice on day 5, they were given 90 seconds to freely swim around the pool. Each mouse's average time spent in TQ was recorded to calculate how long they spent retrieving the concealed platform.

- *Elevated plus maze test*

Two open arms, each extending 16 by 5 cm, and two covered arms, each extending 16 by 5 cm by 15 cm, made up the mouse elevated plus maze.[24] These arms extended outward from a 5 cm by 5 cm platform in the center of the maze, which was 25 cm from the ground. On day one, we arranged the mice in groups, facing away from the central platform, on opposite ends of extended arms. We termed the duration for an animal to use all four legs to travel from the open arm to one of the closed arms a "transfer latency" (TL). The TL of every animal was established on day 1. (the 27th day after medication delivery). After 90 seconds, if the rat still did not climb into its caged arm, it was persuaded and given a 90-second time limit. The mouse was returned to its cage after two additional minutes of labyrinth navigation. This newly learned ability was assessed for memory 24 hours (on day 28) after the first trial.

- *Dissection and homogenization*

After finishing their behavioral testing, the animals were sacrificed. After the brains were removed, they were washed in cold salt water. A phosphate buffer of 0.1 M (pH 7.4) was used for the homogenization. For biochemical analysis, the homogenate was centrifuged.

- *Acetylcholinesterase enzyme biochemical estimation*

The Ellman method was used to determine the amount of acetylcholinesterase, a cholinergic marker, in the whole mouse brain.[25] For a yellow chromophore, the wavelength at which colorimetric measurements are taken is 412 nm (5-mercapto-

2-nitro-bezoic acid). The enzyme level was determined by calculating the rate of rise in absorbance for a period of up to 2 minutes. In a mixture containing 3 mL of phosphate buffer, pH 8, 0.10 mL of Ellman reagent (DTNB), and 0.005 mL of the supernatant, we added 0.10 mL of acetylthiocholine iodide. Hydrolysis rates of substrates were calculated in units of µmoles per minute per mg of protein by monitoring the shift in optical density at 412 nm.

Statistical Analysis

Statistics are often shown as means ± SEM. One-way ANOVA and Tukey's post hoc test for statistical significance were used to examine the differences between the two groups in Graph Pad Prism 5. A statistically significant result was determined when $p < 0.05$.

RESULTS

Extraction and Partitioning

We employed a series of solvent extractions known as maceration to get the plant material ready for extraction. For the subsequent solvent extraction procedure, the maceration technique was employed with the dried, coarsely powdered sample. To extract the methanol from the shade-dried powder, 80 g was macerated in 250 mL of water for one week while stirring occasionally. The crude powder was filtered with Whatman paper no.1, and the methanolic extracts were collected and pooled using the triple maceration procedure. Every time, the drug material that had been ground was left to dry in the open air before being fractionated further. At last, a sticky substance was produced by evaporating the surplus solvent to solventlessness at 37°C under decreased pressure using a rotary evaporator. This material was then kept in a desiccator for subsequent phytochemical analysis. The formula stated below is used to compute the percentage of extractive yield (Figure 1).

Yield% = Dried extract wt. x 100/ Dried crude powder wt.

Yield% =10g x 100/ 80g = 30%

Pet ether, water, and chloroform were used to separate the various fractions of the parent extract, which is a methanolic extract. The methanolic extract was combined with pet ether to isolate lipid and pigment components. Chloroform and water were used to separate the residual extract after the pet. ether fraction was separated. Following this, the gathered portions were dried and given respective labels: Methanolic mother extract (M1), petroleum ether fraction (P1), chloroform fraction (C1), and the hydroalcoholic fraction, which was the residual water fraction (H1).

A B C D

Figure 1: A) Dried crude powder maceration using methanol (B) Filtration of macerates and collection of crude extract (C) Partitioning of methanolic extract using pet ether (D) Partitioning of methanolic extract using chloroform.

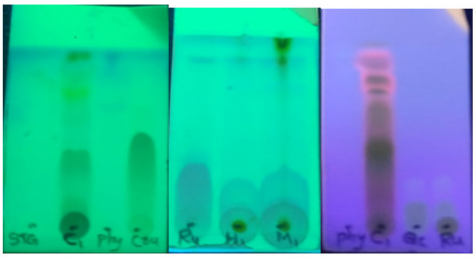

A B C

Figure 2: All TLC ran in mobile phase pet ether: ethyl acetate (3:1)

Phytochemical Screening

We used established protocols to apply the produced fractions and extracts to chemical testing to determine the nature of the phytoconstituents. Table 2 displays the conclusions drawn from the observations.

Chemical Characterization of Extract

TLC studies

The existence of several phytoconstituents, including steroids, terpenoids, glycosides, flavonoids, and phenolic compounds, was investigated in the M1 extract and its fractions C1, P1, and H1 utilizing diverse polar and non-polar solvent systems, following the polarity of the phytocompounds in the samples. A

Table 1: Animal grouping

Group	*Name*	*Treatment*
I	Control group	Saline
II	Diseased group	
III	Low dose group	Extract
IV	High dose group	Extract
V	Standard Group	Glibenclamide (5mg/kg b.w.)

Table 2: Qualitative analysis of prepared *Alternanthera pungens* extract/fractions using chemical tests

S.No	*Phyto constituents*	*M1*	*P1*	*C1*	*H1*
1	Flavonoids	+	-	+	-
2	Alkaloids	+	-	+	+
3	Saponins	+	-	-	+
4	Phenolic compounds or Tannins	+	-	-	+
5	Volatile oils	+	-	+	-
6	Steroids and triterpenoids	+	+	+	+
7	Glycosides	+	-	+	+
8	Anthraquinone	+	-	-	+
9	Protein	+	+	-	+
10	Carbohydrates	+	-	+	+
11	Lipids	+	+	+	-

Whereas M1 is the methanolic extract and P1, C1, and H1 are the fractions of whole parts of *Alternanthera pungens.* "+" indicates presence; "-'' indicates absence of phytoconstituents.

non-polar solvent system including pet ether and ethyl acetate (3:1) stood out above all the others, regardless of the ratio, due to the presence of distinct and important molecules. The chemical testing findings prompted the selection of the C1 fraction for standardization, which was then compared to a small set of reference flavonoidal and terpenoidal substances (Figure 2).

- TLC of C1 in comparison with stigmasterol (STG), phytol (Phy), and quercetin (cru) B) TLC of M1 extract and H1 fractions observed under UV light in comparison with rutin (Ru) C) TLC of C1 extract fraction comparing with quercetin (Qs) and rutin (Ru) and Phytol (Phy) in far UV.

Standardisation by TLC methods

Qualitative examination revealed that methanolic extracts included alkaloids, terpenoids, steroids, glycosides, saponins, fatty acids, and flavonoids; fractionation with chloroform yielded the highest levels of terpenoids and flavonoids since chloroform is a medium polar solvent. A hydro-alcoholic fraction is formed by separating polar molecules, including alkaloids, saponins, terpenoids, carbohydrates, glycosides, and sugars. Chloroform fraction included biologically active heterocyclic flavonoids, terpenoids, and glycosides (C1). Table 3 displays the results of other standardization experiments that used chloroform fraction (C1) data.

Using chemical assays, the chloroform (C1) extract was tested for the presence of several phytocompounds (Table 2).

The mobile phases used in thin-layer chromatography included mixtures of methanol and dimethylamine, ethyl acetate, toluene, and dimethylamine, as well as pet ether and ethyl acetate. Using a mobile phase of pet ether: ethyl acetate (3:1), the M1 mother crude extract and its C1, P1, and H1 fractions were analyzed using a thin-layer chromatography (TLC) technique. The results were seen under near-UV light and with the spraying reagent PMA. This information is shown in Figure 3, along with a few reference compounds.

The findings of the TLC experiments indicated that, in comparison to the standard chemicals stigmasterol, quercetin (a flavonoid compound), and rutin (a flavonoid glycoside), quercetin and rutin were detected in the methanol fraction (C1) (fattysterol). Using a mobile phase of pet ether: ethyl acetate (3:1), the existence of rutin was verified by TLC as shown in Figures 3C and D. Additionally, the presence of rutin was established using PMA stain (as a visualizing agent) at an Rf value of 0.86 and quercetin at 0.65. Additional research using HPTLC is necessary to standardize the bioactive chloroform component and methanolic extracts.

Standardisation by HPTLC technique

The crude methanol extract and its fractions were standardized with quercetin and rutin using the HPTLC technique (Table 3 and Figure 3).

According to the data tables provided, the methanolic extract exhibited a high number of bands (13–14) when

Table 3: HPTLC Fingerprint of methanol extracts of *A. pungens*

Component	*UV 254 nm Rf value*	*Linearity range (ng/spot)*
Methanol extraction(M)	0.175	200-1400
Aqueous methanol fraction(H)	-	200-1400
Chloroform fraction (C)	0.18	200-1400
Quercetin (Q)	0.18	200-1400
Rutin (R)	0.16	200-1400

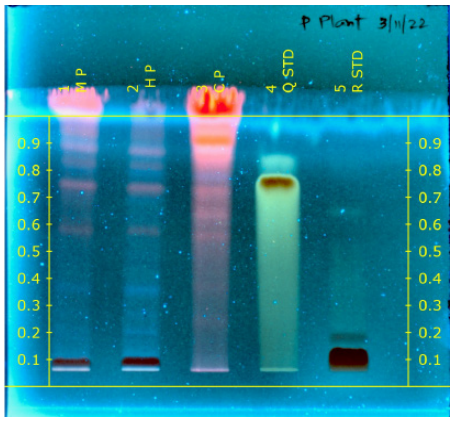

Figure 3: HPTLC fingerprint profile of methanol extract test sample (MP), hydroalcoholic fraction test sample (HP), chloroform fraction (CP), quercetin (Q STD) rutin (R STD)

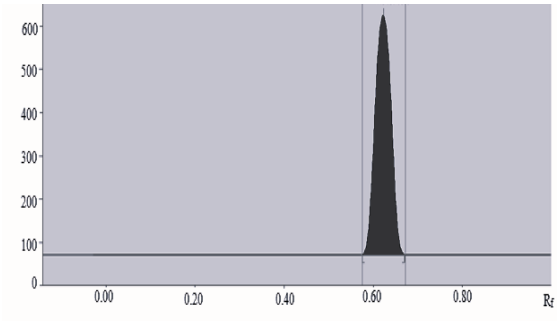

Figure 4: HPTLC chromatogram of qucertein

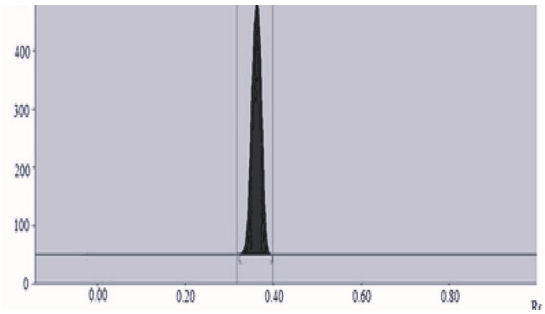

Figure 5: HPTLC Chromatogram of rutin

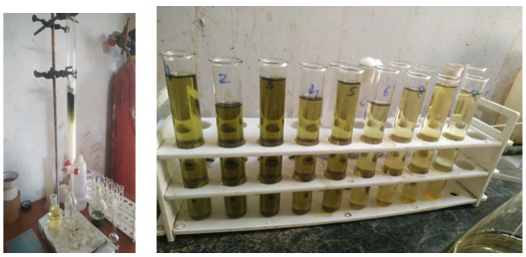

Figure 6: Column chromatography of *A. pungens* chloroform extract

exposed to ultraviolet light, suggesting the presence of several phytoconstituents. Under UV 254 nm, the hydroalcoholic fraction did not exhibit any bands. There are seven or eight bands visible in the chloroform residue. Among all of them, the chloroform fraction and reference quercetin have Rf values of 0.9 under UV 254 nm for the 4th band from the baseline; the methanolic extract, on the other hand, is very close to standard quercetin and rutin, with Rf values of 0.75, 0.9, and 0.1. Accordingly, the HPTLC approach also revealed the presence of Quercetin and Rutin (Figure 4 and 5).

Isolation of compounds from selected chloroform fraction of A. pungens

To prepare the material to be adsorbed in the silica gel, 1-gm of dried chloroform fraction of *A. pungens* was combined with 10 gms of silica gel (60–120 mesh). From a starting point of one hundred percent pet ether, the column was eluted with solvents ranging from (0–100%) ethyl acetate in pet ether, with a total of 90 fractions recovered. We used thin-layer chromatography (TLC) to examine each of the obtained fractions after we evaporated the solvents in a water bath (Figure 6).

Isolation and purification of the compound

The combinations of identical fractions were determined by the Rf values. The pools that produced a single spot when exposed to UV light were fractions 8–16. A final yield of around 85 mg of compound A was achieved by combining and evaporating 8 to 16 portions to produce a liquid compound. The process of column chromatography was performed continuously using a mixture of dichloromethane and MeOH. The collected fractions 25–32 were likewise crystallized to yield 70 mg of chemical B. To get the amount of compound B needed, the fraction-combining and crystallization procedure was performed several times, each time with a bigger sample size (Figure 7).

Characterization of isolated compounds A&B

- *Compound A*

The product is a loose, yellow powder with a melting point of 316.3°C and a yield of 70 mg (1.4% by weight). The schinoda test revealed a pink hue, whereas the ferric chloride test revealed a blue-green hue. Substance A has been identified as a flavonoid. Spraying using a PMA reagent produced in petroleum ether: ethyl acetate (7:3) solvent solution resulted in blue color spots, according to TLC examinations. The computed Rf value is 0.54. Compound A's absorption peaks at 401 and 261 nanometers in its UV-spectra observed in methanol. Compound A's measured infrared spectra are shown in Figure 8. These findings may help with the identification and characterization of chemical A by providing information about the functional groups it contains.

Figure 8, the infrared (IR) spectrum of compound A was analyzed and several characteristic absorption bands were observed. A peak at 3288.04 cm^{-1} was identified as the stretching vibration of the hydroxyl group (-OH) in phenol. Another peak at 1613.23 cm^{-1} was assigned to the stretching vibration of the carbon-carbon (C-C) bond in the aromatic ring. The absorption band at 1245.53 cm^{-1} was attributed to the stretching vibration of the carbon-oxygen (C-O) bond in the aryl ether functional group.

In addition, the stretching and bending vibrations of the carbon-oxygen-carbon (C-O-C) bond in the ketone group were attributed to a peak at 1141.71 cm {-1. Lastly, the aromatic hydrocarbon's carbon-hydrogen (C-H) bond bending vibrations were attributed to two bands at 822.28 and 612.01 cm^{-1}. A molecular ion peak [M+1]+ at m/z 303.0514 was detected in the positive ion ESI-MS study of chemical A, as seen in Figure 8. Insights into chemical A's molecular weight and formula, as revealed by this data, may greatly facilitate its identification and characterization (Figure 9).

Nuclear magnetic resonance (NMR) analyses verified the locations of carbon and proton binding sites. An improved resolution in the ^{1}H-NMR spectra was observed for the isolated chemical A. Figures 10 and 11 shows the ^{1}H-NMR spectra of the released chemical, which disclosed aromatic hydrogen groups at 6.19 to 7.68 ppm and phenolic-OH groups at 9.32 to 12.50 ppm. Standard Quercetin, a hydrocarbon with the molecular formula C15H10O7, has all these notable bonds that are compatible with it. Therefore, compound A was identified as quercetin in Table 4.

- *Compound B*

This compound is obtained as a clear liquid and a yield of 85 mg (1.7% by weight). The Libermann butchard test turned it red, the Salkowski test turned it no green, and the ferric chloride test turned it blue-green. The flavonoidal glycoside status of compound B has been established. According to TLC experiments, a blue spot appears when the PMA reagent is sprayed using a solvent solution consisting of a 9:1 ratio of dichloromethane to methanol. The stretching vibration of the hydroxyl (-OH) group was apparent in the IR spectra of rutin, which displayed a wide and strong absorption band at 3,435 cm^{-1}. Seeing a prominent peak at 1,041 cm^{-1}, which is suggestive of the C-O stretching vibration, further demonstrated the existence of a hydroxyl group. The presence of a distinct peak at 1,629 cm^{-1} suggests that the flavone ring is vibrating due to the C=C stretching vibration. Furthermore, a band of medium strength at 1,173 cm^{-1} was seen, which is thought to be caused by the stretching vibration of the glycosidic bond C-O-C. There was evidence of C-H bending vibration in the aromatic ring at 1,386 cm^{-1}.

In general, rutin's infrared spectra showed that the compound had hydroxyl groups, a flavone ring, and a glycosidic bond. The findings align with the established chemical formula of rutin as a flavonoid glycoside, as seen in Figure 12. Compound A's ESI-MS (positive ion mode) results in Figure 13 displayed a [M+1]+ peak at m/z 611.36 and a [M-1]+ peak at 609.38, indicating molecular ions

As seen in Table 5, rutin and isolated compound B both have ^{1}H and ^{13}C-NMR resonances. Table 5 compares the two compounds' chemical shifts for different carbon atoms. Two columns are provided: one with the carbon numbers and another with the chromophores that correspond to those numbers. Isolated compound B's and rutin's ^{1}H-NMR chemical shifts (in

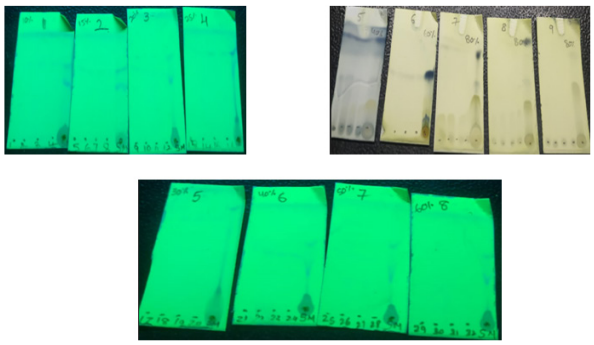

Figure 7: Detection of isolates: (A) Isolation of compd-A using near UV (B) Isolation of compd-A using near UV (C) Isolation of compd-B using PMA Stain

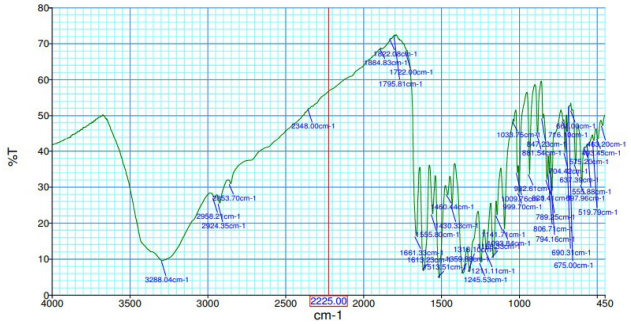

Figure 8: Isolated compound–quercetin-IR spectrum

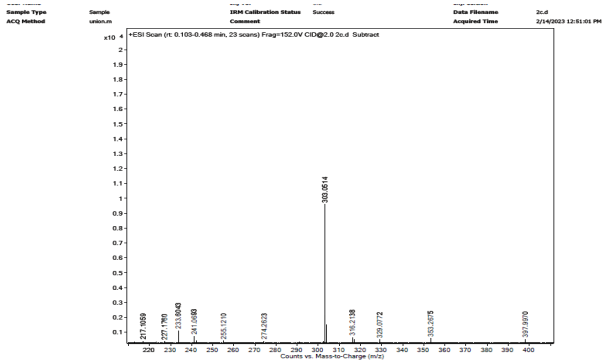

Figure 9: Isolated compound–quercetin-mass spectrum

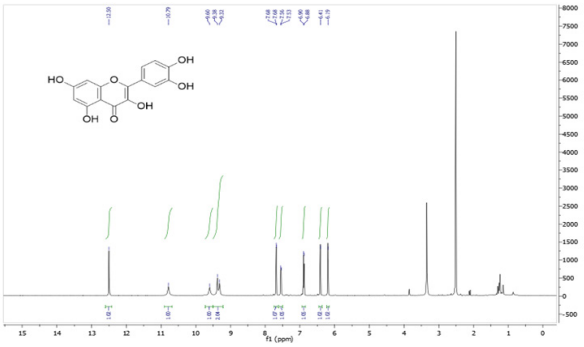

Figure 10: Isolated compound–$^{A\text{-}1}$H NMR spectrum

Table 4: ^{1}H and ^{13}C-NMR Resonances of Quercetin and Isolated Compound A

Carbon No.	*Chromophore*	*Quercetin 1HNMR Chem Shifts a (ppm)*	*Compound A 1H NMR Chem Shifts a (ppm)*	*Quercetin 13C NMR Chem Shifts b (ppm)*	*Compound A 13C NMR Chem Shifts b (ppm)*
1	C-1	12.16 (s)	-	177.2	176.30
2	C-2	6.88 (d, J = 8.7 Hz)	7.68 (d, J = 1.8 Hz, 1H)	158.8	156.60
3	C-3	7.50 (d, J = 2.1 Hz), 6.97 (d, J = 8.7 Hz)	6.89 (d, J = 8.5 Hz, 1H)	93.9	93.80
4	C-4	6.55 (d, J = 2.1 Hz)	-	160.4	161.19
5	C-5	7.57 (dd, J = 8.7, 2.1 Hz)	-	99.3	98.64
6	C-6	6.98 (d, J = 8.7 Hz)	-	157.7	156.60
7	C-7	7.86 (d, J = 8.7 Hz)	-	121.5	120.43
8	C-8	6.81 (d, J = 8.1 Hz)	6.41 (s, 1H)	145.4	145.52
9	C-9	7.47 (d, J = 2.1 Hz), 6.99 (d, J = 8.7 Hz)	6.19 (s, 1H)	94.1	93.80
10	C-10	6.01 (d, J = 1.8 Hz), 6.18 (d, J = 1.8 Hz)	-	105.9	103.47
11	C-1’	6.77 (d, J = 2.1 Hz)	-	115.3	115.53
12	C-2’	7.56 (dd, J = 8.4, 2.1 Hz)	-	131.9	136.19
	C-3’	7.47 (d, J = 8.1 Hz)		114.2	115.53
	C-4’	6.80 (d, J = 8.1 Hz)		152.7	156.60
	C-5’	6.80 (d, J = 8.1 Hz)		118.8	116.06
	C-6’	7.56 (dd, J = 8.4, 2.1 Hz)		145.6	145.52
	C-7’	7.56 (dd, J = 8.4, 2.1 Hz)			

a 500MHz, CDCl3, b 125 MHz, CDCl3

ppm) are shown in the adjacent two columns, correspondingly. The 13C NMR chemical shifts of the compounds presented in Figure 14 are shown in the final two columns. These significant bonds are consistent with the molecular formula of the common hydrocarbon rutin (C27H30O16). Compound B was therefore identified as rutin.

Following its isolation and analysis by ^{13}C-NMR, Compound B showed a high degree of resonance congruence with the ^{13}C-NMR chemical shift assignments of rutin. Particularly, the ^{13}C-NMR resonances at 59.39, 123.09, and 140.23 ppm for carbons 1–3 of rutin were determined to correlate to the analogous resonances at 59.3, 123.18, and 140.04 ppm, correspondingly, of compound A. Compound B is rutin, as shown by additional peaks at 39.88, 39.37, 37.53-37.19, 36.68, 32.74, 29.70, 27.97, 25.14, 24.79, 24.47, 22.66, 19.72, and 16.14 in compound A's ^{13}C-NMR resonances (Figure 15). According to the table, rutin and isolated compound B share a similar chemical composition as their carbon atoms undergo relatively comparable chemical changes. Nevertheless, certain carbon atoms in isolated compound A have different chemical shifts compared to their equivalent resonances in rutin. These carbon atoms include C-7, C-8, C-9, C-3', and C-5'.

To identify and characterize isolated compound A'wwvs chemical structure, the data presented in the preceding table is vital. This table contains chemical shifts that may be utilized for analyzing the spectra of rutin and isolated compound A using nuclear magnetic resonance (NMR) spectra, which are often employed in natural product research to elucidate structures.

Chromophore: Each carbon's corresponding chromophore is listed in this column. Carbon atoms in the flavonoid ring structure are denoted by the "C" chromophore, and carbon atoms in the glucose and rhamnose molecules are denoted by the "G" and "R" chromophores, correspondingly.

Rutin ^{1}H-NMR (ppm): Here we can see the ^{1}H-NMR spectral data for each proton in rutin, along with its associated chemical shift (in ppm). A proton on carbon 2 in rutin, for instance, presents as a pair possessing a coupling constant of 2.0 Hz and a chemical shift of 6.21 ppm.

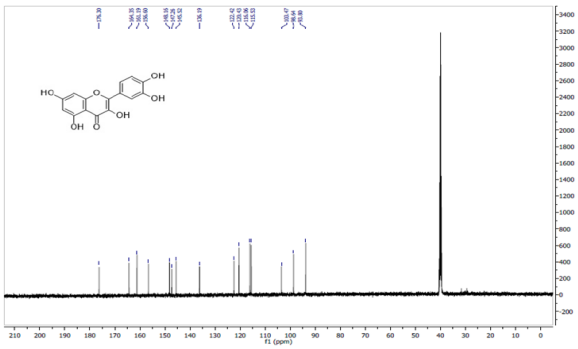

Figure 11: Isolated Compound-A-^{13}C NMR Spectrum

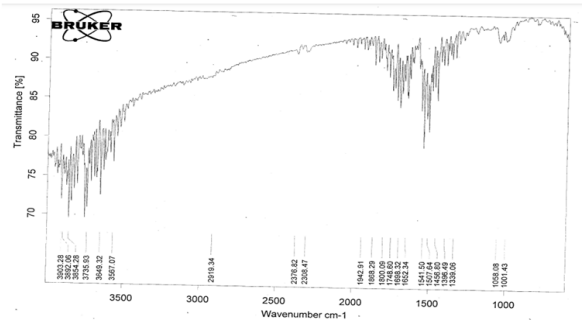

Figure 12: IR Spectrum-compound-B

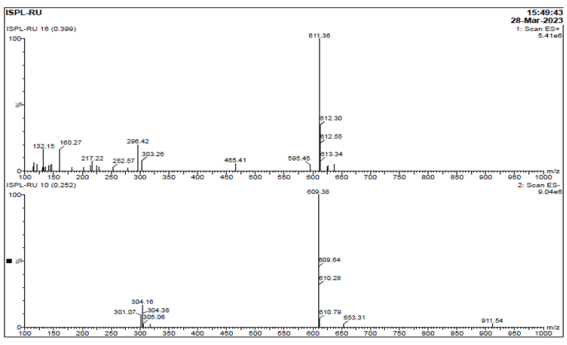

Figure 13: Mass Spectrum-compound-B

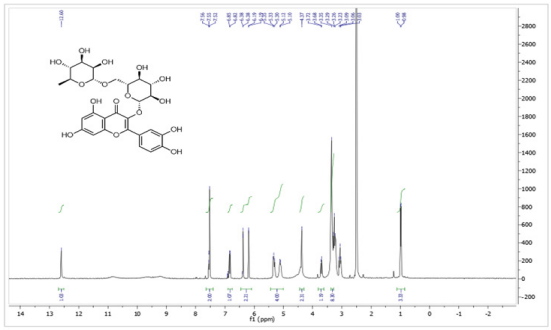

Figure 14: ^{1}H-NMR Spectrum-compound-B

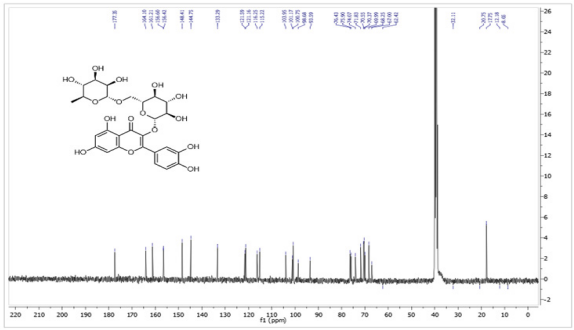

Figure 15: ^{13}C-NMR Spectrum-compound-B

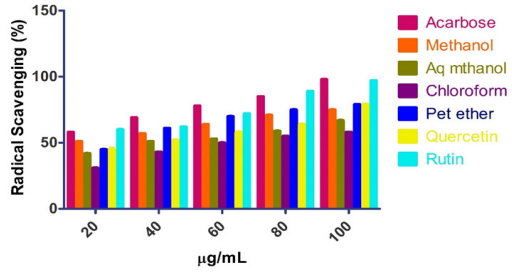

Figure 16: *In-vitro* alpha-amylase inhibitory activity of *Alternanthera Pungens*

Compound B ^{1}H-NMR (ppm): Compound B's associated proton's ^{1}H-NMR spectral shift is listed in this column, along with the related chemical shift in ppm. As an example, the proton bonded to carbon 2 in compound B exhibits a 6.19 ppm chemical shift and manifests as a pair of doublets having coupling constants of 57.4 and 2.0 Hz.

Rutin ^{13}C-NMR (ppm): Based on ^{13}C-NMR spectroscopic measurements, this column shows the chemical shift (in ppm) of the equivalent carbon in rutin. The chemical shift of the carbon 2 atom in rutin, for instance, is 157.3 ppm.

Compound B ^{13}C-NMR (ppm): Compound B's associated carbon chemical shift, as determined by ^{13}C-NMR spectroscopy, is listed in this column. The shift is expressed in parts per million. A chemical shift of 156.60 ppm is seen, for instance, for the carbon 2 atom in compound B.

Selection of Suitable Solvent

In-vitro anti-amylase activity of A. pungens

Rutin and methanolic extract were shown to have a greater percentage of amylase activity suppression compared to aq methanolic, chloroform, pet ether extract, and quercetin. Results showed that the IC_{50} for methanolic extract was 17, and for rutin, it was 8.7 µg/mL; for aq methanol, chloroform, pet ether, and quercetin they were 45, 68, 21, and 35 µg/mL, correspondingly (Table 6 and Figure 16).

In-vitro glucosidase inhibitory activity of A. pungens

Rutin and methanolic extract had a greater percentage of glucosidase activity suppression compared to quercetin, chloroform, pet ether, and aq methanolic extract. Aq methanol, chloroform, pet ether, and quercetin had IC_{50} values of 49, 45, 25, and 29 µg/mL, correspondingly, whereas rutin and methanolic extract had IC_{50} values of 12 and 6.2 µg/mL, respectively (Table 7 and Figure 17).

Evaluation of Antidiabetic Activity

Effect of MEAP on oral glucose tolerance test

While the normal control group had mean OGTT levels of 224 ± 7.2 mg-h/dL, the diabetes control group had levels of 593 ± 3.7 mg-h/dL, a statistically and clinically significant increase ($p < 0.001$). When these elevated levels were treated with MEAP and glibenclamide, the findings were statistically significant ($p < 0.001$), (Figure 18, 19, and Table 8). Table 8 shows the reported glucose levels at different times.

Table 5: ^{1}H and ^{13}C-NMR resonances of rutin and isolated compound B

Carbon No.	*Chromophore*	*Rutin ^{1}H-NMR (ppm)*	*Compound B ^{1}H-NMR (ppm)*	*Rutin ^{13}C-NMR (ppm)*	*Compound B ^{13}CNMR(ppm)*
C-2	C	6.21 (d, J = 2.0 Hz, 1H)	6.19 (dd, J = 57.4, 2.0 Hz)	157.3	156.60
C-3	C	6.40 (d, J = 2.0 Hz, 1H)	6.38 (dd, J = 57.4, 2.0 Hz,2H)	134.1	133.29
C-4	C			178.2	177.35
C-5	C			157.5	156.60
C-6	C	5.35 (d, J = 7.4 Hz, 1H)	5.01-5.43 (m, 4H)	99.5	98.68
C-7	C		10.86 (s, 1H)	164.9	164.10
C-8	C	6.86 (d, J = 9.0 Hz, 1H)	6.85 (t, J = 8.7 Hz, 1H)	94.5	133.29 93.59
C-9	C	7.55 (d, J = 2.1 Hz, 1H)	7.64–7.40 (m, 2H)	162.1	161.21
C-10	C			104.8	103.95
C-1'	C	7.56 (dd, J = 9.0, 2.1 Hz, 1H)		122.5	121.59
C-2'	C	7.55 (d, J = 2.1 Hz, 1H)		116.1	115.22
C-3'	C	6.86 (d, J = 9.0 Hz, 1H)		145.6	103.95 144.75
C-4'	C			149.3	148.41
C-5'	C	6.40 (d, J = 2.0 Hz, 1H)		117.1	100.75 116.25
C-6'	C	6.21 (d, J = 2.0 Hz, 1H)		122.0	98.68 121.16
C-1G	G	5.12 (d, J = 1.9 Hz, 1H)		101.6	93.59 101.17
C-2G	G			74.9	74.07
C-3G	G			77.3	75.90 76.43
C-4G	G			72.7	71.83
C-5G	G			76.7	76.43
C-6G	G			67.9	70.55
C-1R	R	12.62 (1H, s, C5-OH)	12.60 (s, 1H)	102.2	101.17

Signals from the rhamnose and glucose subunits are denoted by R and G, correspondingly. a 500MHz, CDCl3, b 125 MHz, CDCl3

The results were examined with 6 rats within every group, and shown as the mean ± SEM. $^{\alpha}p < 0.001$, with respect to the NC group; $^{a}p < 0.001$, with respect to the DC group.

- *Effect of MEAP on serum glucose levels*

Throughout the course of the investigation, the diabetic control group's BGLs rose significantly. Serum glucose levels in the diabetes control group were 308 ± 9.1 mg/dL after the research, which was substantially greater than the NC group ($p < 0.001$). When MEAP and glibenclamide were used to treat the high blood glucose level, it was reduced dramatically ($p < 0.001$) (Figure 20 and Table 9).

The outcomes were examined with six rats within every group, and shown as the mean ± SEM. $^{\alpha}p < 0.001$, with respect to the NC group; $^{a}p < 0.001$, $^{b}p < 0.01$, and $^{c}p < 0.05$, with respect to the DC group.

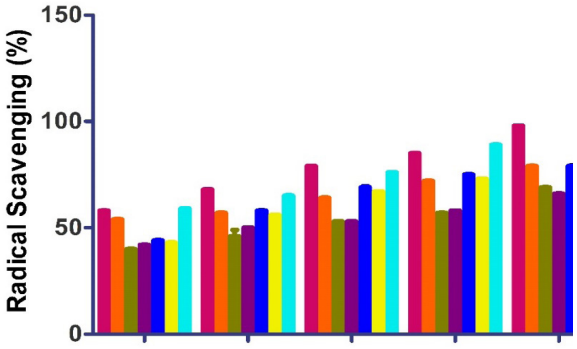

Figure 17: *In-vitro* glucosidase inhibitory activity of *A. pungens*

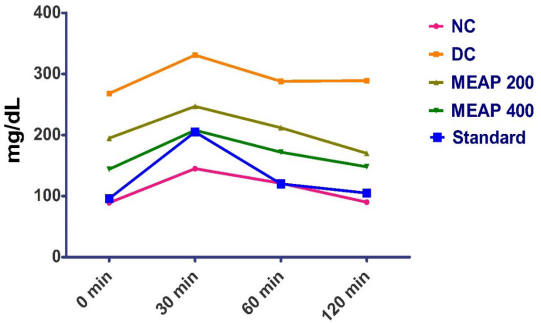

Figure 18: Effect of MEAP on OGTT

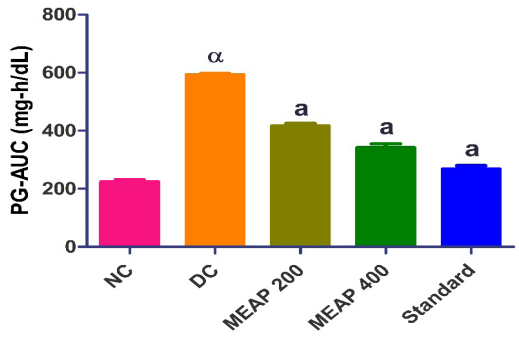

Figure 19: Effect of MEAP on AUC

Effect of MEAP on lipid parameters

- *Triglyceride levels*

The normal control group had a mean serum triglyceride level of 69 ± 3.8 mg/dL, whereas the diabetes control group's level was 125 ± 3.3 mg/dL, a statistically and clinically significant difference ($p < 0.001$) (Table 10). When MEAP and glibenclamide were used to treat the elevated blood triglyceride level, the levels dropped significantly ($p < 0.001$) (Figure 21 and Table 10).

The findings were examined with 6 rats within every group, and shown as the mean ± SEM. $^{\alpha}p < 0.001$, with respect to the NC group; $^{a}p < 0.001$, with respect to the DC group.

- *Cholesterol levels*

As against NC group's serum total cholesterol level of 78 ± 3.8 mg/dL, the diabetes control group's level of 158 ± 5.7 mg/dL was statistically and clinically significant ($p < 0.001$). Total cholesterol levels were reduced by MEAP 400

Table 6: IC_{50} value of inhibition of alpha-amylase activity of *A. Pungens*

Conc. (µg/mL)	*20*	*40*	*60*	*80*	*100*	*IC_{50}*
Acarbose	58 ± 0.033	69 ± 0.067	78 ± 0.058	85 ± 0.033	98 ± 0.033	2.5 ± 0.068
Methanol	51 ± 0.18	57 ± 0.12	64 ± 0.088	71 ± 0.12	75 ± 0.18	17 ± 0.43
Aq methanol	42 ± 0.061	51 ± 0.12	53 ± 0.088	59 ±0.033	67 ± 0.12	45 ± 0.25
Chloroform	31 ± 0.18	43 ± 0.12	50 ± 0.10	55 ± 0.12	58 ± 0.12	68 ± 0.26
Pet ether	45 ± 0.12	61 ± 0.15	70 ± 0.088	75 ± 0.15	79 ± 0.058	21 ± 0.28
Quercetin	45 ± 1.0	52 ± 0.21	58 ± 0.35	64 ± 0.25	79 ± 0.35	35 ± 0.74
Rutin	60 ± 0.27	62 ± 0.12	72 ± 0.088	89 ± 0.088	97 ± 0.058	8.7 ± 0.46

Alternanthera pungens, IC_{50}: Inhibitory concentration, values are expressed as mean + SEM.

Table 7: IC_{50} value of inhibition of glucosidase activity of *A. Pungens*

Extract	*20*	*40*	*60*	*80*	*100*	*IC_{50}*
Acarbose	58 ± 0.088	68 ± 0.17	79 ± 0.12	85 ± 0.22	98 ± 0.088	2.9 ± 0.022
Methanol	54 ± 0.067	57 ± 0.19	64 ± 0.34	72 ± 0.26	79 ± 0.19	12 ± 0.26
Aq methanol	40 ± 0.21	46 ± 3.0	53 ± 0.088	57 ±0.088	69 ± 0.12	49 ± 0.53
Chloroform	42 ± 0.058	50 ± 0.12	53 ± 0.12	58 ± 0.058	66 ± 0.12	45 ± 0.23
Pet ether	44 ± 0.22	58 ± 0.21	69 ± 0.58	75 ± 0.24	79 ± 0.28	25 ± 0.64
Quercetin	43 ± 0.28	56 ± 0.088	67 ± 0.058	73 ± 0.088	76 ± 0.088	29 ± 0.38
Rutin	59 ± 0.088	65 ± 0.35	76 ± 0.12	89 ± 0.15	98 ± 0.033	6.2 ± 0.47

Alternanthera pungens, IC_{50}: Inhibitory concentration, values are expressed as mean + SEM,

Table 8: Effect of MEAP on OGTT

Groups	*0 min*	*30 min*	*60 min*	*120 min*	*AUC*
NC	89 ± 4.6	145 ± 4.3	121 ± 3.8	90 ± 3.6	224±7.2
DC	268 ± 9.5$^{\alpha}$	331 ± 3.8$^{\alpha}$	288 ± 4.4$^{\alpha}$	289 ± 5.5$^{\alpha}$	593 ± 3.7$^{\alpha}$
MEAP 200	195 ± 7.6^{a}	247 ± 6.8^{a}	212 ± 7.5^{a}	170 ± 7.0^{a}	416 ± 8.4^{a}
MEAP 400	144 ± 9.7^{a}	208 ± 5.8^{a}	172 ± 7.6^{a}	148 ± 7.0^{a}	343 ± 13^{a}
Standard	96 ± 5.8^{a}	205 ± 13^{a}	120 ± 1.8^{a}	105 ± 4.1^{a}	269 ± 11^{a}

Table 9: Effect of MEAP on serum glucose levels

Day	*NC*	*DC*	*MEAP 200*	*MEAP 400*	*Standard*
0	97 ± 7.9	281 ± 9.4	286 ± 7.2	282 ± 9.1	284 ± 11
7	98 ± 8.0	290 ± 9.2$^{\alpha}$	253 ± 7.8^{c}	228 ± 10^{a}	223 ± 7.5^{a}
14	99 ± 8.1	296 ± 9.7$^{\alpha}$	201 ± 7.8^{a}	155 ± 6.9^{a}	140 ± 4.8^{a}
21	101 ± 6.9	302 ± 9.5$^{\alpha}$	195 ± 12^{a}	142 ± 8.0^{a}	124 ± 8.3^{a}
28	102 ± 6.7	308 ± 9.1$^{\alpha}$	149 ± 8.8^{a}	119 ± 9.9^{a}	108 ± 8.0^{a}

The findings were examined with six rats within every group, and shown as the mean ± SEM. $^{\alpha}p < 0.001$, with respect to the NC group; $^{a}p < 0.001$ and $^{c}p < 0.05$, with respect to the DC group.

Table 10: Effect of EEHS on serum lipid profile

Para meters	*NC*	*DC*	*MEAP 200*	*MEAP 400*	*Standard*
TG (mg/dL)	69 ± 3.8	125 ± 3.3$^{\alpha}$	96 ± 3.2^{a}	81 ± 4.0^{a}	81 ± 3.7^{a}
TC (mg/dL)	78 ± 3.8	158 ± 6.7$^{\alpha}$	141 ± 2.8	125 ± 5.5^{a}	86 ± 3.8^{a}
HDL (mg/dL)	27 ± 1.6	12 ± 1.1$^{\alpha}$	19±0.99^{b}	24 ± 1.3^{a}	26 ±0.97^{a}

The findings were examined with 6 rats within every group, and shown as the mean ± SEM. $^{\alpha}p < 0.001$, with respect to the NC group; $^{a}p < 0.001$ and $^{b}p < 0.01$ with respect to the DC group.

and glibenclamide therapy relative to the diseased group ($p < 0.001$), however, no significant reduction was noted in total cholesterol levels with MEAP 200 treatment (Figure 22 and Table 10).

The findings were examined with 6 rats within every group, and shown as the mean ± SEM. $^{\alpha}p < 0.001$, with respect to the NC group; $^{a}p < 0.001$, with respect to the DC group.

- *HDL-c levels*

Serum HDL-cholesterol levels dropped significantly ($p < 0.001$) from 27 ± 1.6 to 12 ± 1.1 mg/dL in the diabetes induction group as against the normal control group (Table 10). A substantial rise in blood HDL-c levels was seen in the treatment groups that received MEAP 200, MEAP 400, and glibenclamide, relative to the diabetes control group ($p < 0.01$, $p < 0.001$, and $p < 0.001$) (Figure 23 and Table 10).

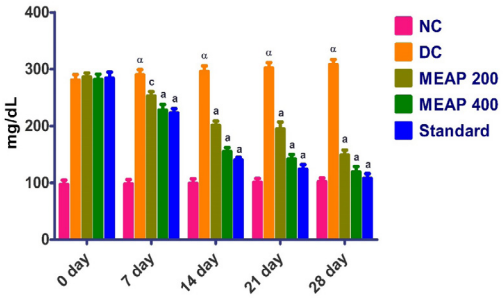

Figure 20: Effect of MEAP on serum glucose levels

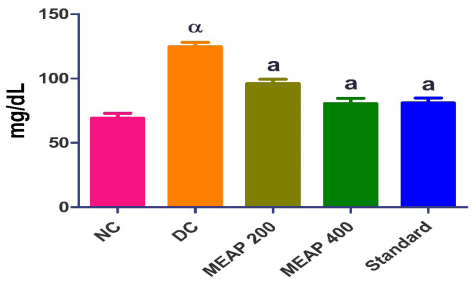

Figure 21: Effect of MEAP on TG levels

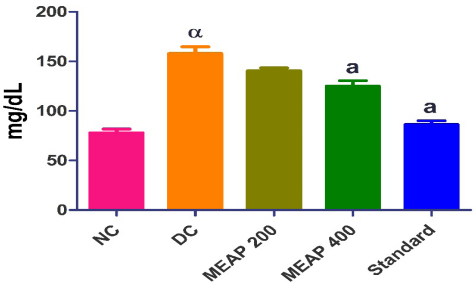

Figure 22: Effect of MEAP on TC levels

The findings were examined with 6 rats within every group, and shown as the mean ± SEM. $^{\alpha}p < 0.001$, with respect to the NC group; $^{a}p < 0.001$ and $^{b}p < 0.01$ with respect to the DC group.

Effect of MEAP on liver parameters

- *SGOT levels*

The normal control group had liver SGOT levels of 43 ± 3.7 U/L, whereas the induction of hyperglycemia led to a substantial ($p < 0.001$) rise to 169 ± 6.9 U/L. The use of MEAP and glibenclamide resulted in a lowering of the elevated SGOT levels ($p < 0.001$) (Figure 24 and Table 11).

The findings were examined with 6 rats within every group, and shown as the mean ± SEM. $^{\alpha}p < 0.001$ with respect to the NC group; $^{a}p < 0.001$ with respect to the DC group.

- *SGPT levels*

Liver SGPT levels increased significantly ($p < 0.001$) from 20 ± 2.8 U/L to 168 ± 5.1 U/L after diabetes induction, as against NC group (Table 11). The elevated SGPT levels were reduced when administered MEAP 200, MEAP 400, and glibenclamide ($p < 0.01$, $p < 0.001$, and $p < 0.001$) therapy (Figure 25 and Table 11).

Table 11: Effect of MEAP on liver parameters

Group	*SGOT (U/L)*	*SGPT (U/L)*
NC	43 ± 3.7	20 ± 2.8
DC	169 ± 6.9$^{\alpha}$	168 ± 5.1$^{\alpha}$
MEAP 200	111 ± 6.8^{a}	138 ± 4.3^{b}
MEAP 400	102 ± 5.7^{a}	85 ± 5.6^{a}
Standard	57 ± 3.6^{a}	57 ± 5.0^{a}

The findings were examined with 6 rats within every group, and shown as the mean ± SEM. $^{\alpha}p < 0.001$, with respect to the NC group; $^{a}p < 0.001$ and $^{b}p < 0.01$ with respect to the DC group.

Table 12: Effect of MEAP on behavioral parameters in Morris water maze

Groups	*Escape latency (s)*					*TSTQ*
	Day 1	*Day 2*	*Day 3*	*Day 4*	*Day 5*	
NC	75 ± 0.91	68 ± 1.1	59 ± 0.69	44 ± 1.4	36 ± 1.0	27 ± 1.2
DC	84 ± 1.1$^{\alpha}$	82 ± 1.1$^{\alpha}$	79 ± 1.6$^{\alpha}$	81 ± 1.2$^{\alpha}$	73 ± 1.6$^{\alpha}$	6.7 ± 0.88$^{\alpha}$
MEAP 200	78 ± 0.82^{b}	77 ± 0.74	75 ± 2.0	61 ± 2.3^{a}	54 ± 1.7^{a}	14 ± 1.5^{a}
MEAP 400	76 ± 0.99^{b}	74 ± 0.98^{a}	68 ± 2.0^{a}	51 ± 1.9^{a}	41 ± 1.6^{a}	19 ± 1.5^{a}
Standard	76 ± 1.2^{a}	68 ± 1.2^{a}	61 ± 1.6^{a}	47 ± 0.48^{a}	37 ± 1.2^{a}	25 ± 2.6^{a}

The findings were examined with 6 rats within every group, and shown as the mean±SEM. $^{\alpha}p < 0.001$, as against the NC group; $^{a}p < 0.001$ and $^{b}p < 0.01$, relative to DC group.

Table 13: Effect of EEFP on TL on EPM test

Group	*TL (sec) on the 0th day*	*TL (sec) on 28th day*
NC	24 ± 1.1	18 ± 1.5
DC	23 ± 1.1	29 ± 1.8$^{\alpha}$
MEAP 200	20 ± 1.6	23 ± 1.3^{c}
MEAP 400	23 ± 1.6	20 ± 1.2^{b}
Standard	20 ± 1.2	19 ± 1.2^{a}

The findings were examined with 6 rats within every group, and shown as the mean±SEM. $\alpha p < 0.001$, relative to the NC group; $ap < 0.001$, $bp < 0.01$, and $cp < 0.05$, relative to DC group.

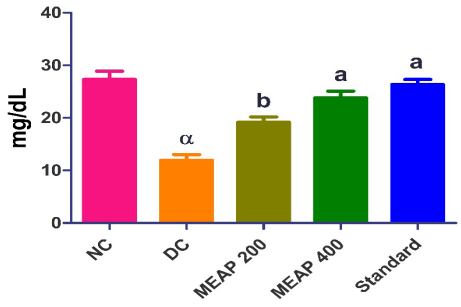

Figure 23: Effect of MEAP on HDL levels

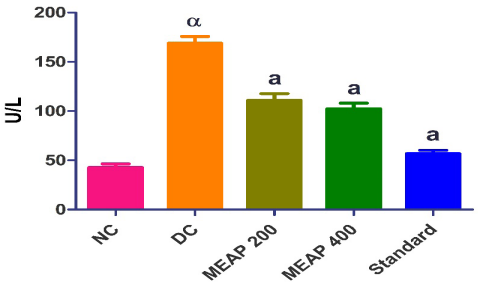

Figure 24: Effect of MEAP on SGOT levels

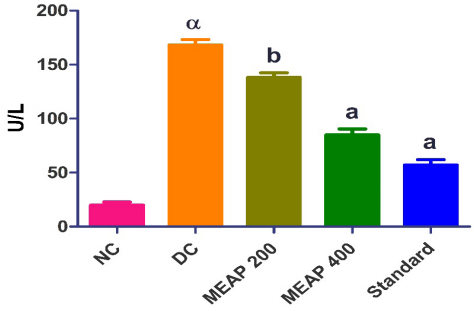

Figure 25: Effect of MEAP on SGPT levels

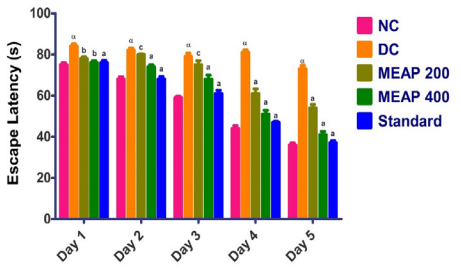

Figure 26: Effect of EEFP on Escape Latency on Morris Water Maze

The findings were examined with 6 rats within every group, and shown as the mean ± SEM. $^{\alpha}p < 0.001$, with respect to the NC group; $^{a}p < 0.001$ and $^{b}p < 0.01$ with respect to the DC group.

Evaluation of behavioral parameters

- *Effect of MEAP in Morris water maze*

Across all five days of testing, the DC group showed significantly shorter escape latencies than the NC group ($p < 0.001$). On day one of treatment with MEAP 200, the animals' escape delay significantly rose as against the DC group ($p < 0.01$); however, this impact was decreased on days two and three of testing. On the fourth and fifth day after MEAP 200 administration, an increase in escape latency was noted. The escape latency of mice treated with MEAP 400 was significantly longer than the DC group's latency over all five days of the trial ($p < 0.01$, $p < 0.001$, $p < 0.001$, and $p < 0.001$), as was the escape latency of mice treated with the standard medication across all five days of the study ($p < 0.001$) (Table 12 and Figure 26).

When contrasted with the NC group, the length of time spent in TSTQ was significantly declined ($p < 0.001$) due to the induction of Alzheimer's. The TSTQ scores showed a

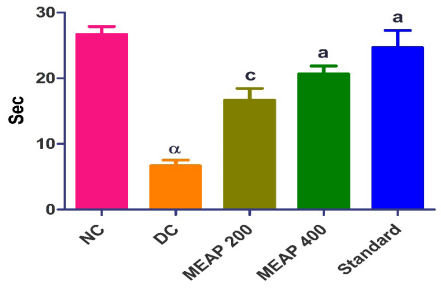

Figure 27: Effect of MEAP on the time spent in the TQ

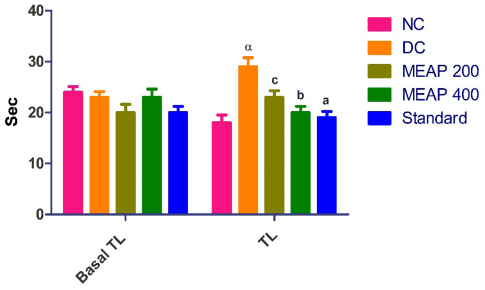

Figure 28: Effect of MEAP on transfer latency

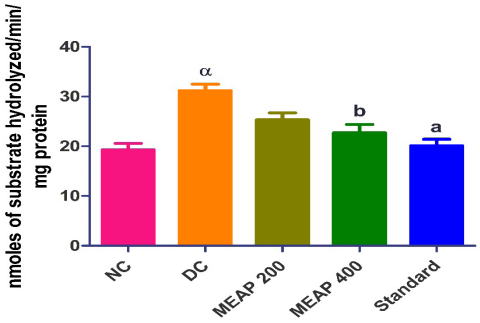

Figure 29: Effect of EEFP on the brain ache levels

substantial improvement in comparison to the DC group in all treated group ($p < 0.001$) (Table 12 and Figure 27).

Each group's data (Mean ± SEM) was based on measurements taken from six rats, and the results were compared. $^{\alpha}p < 0.001$, relative to the NC group; $^{a}p < 0.001$, $^{b}p < 0.01$, as against diabetic group

The findings were examined with 6 rats within every group, and shown as the mean ± SEM. $^{\alpha}p < 0.001$, relative to the NC group; $^{a}p < 0.001$ and $^{c}p < 0.05$, relative to DC group.

- *Effect of MEAP on EPM*

Relative to the control group, the DC group displayed a much longer transfer latency ($p < 0.001$). The MEAP 200, MEAP 400, and Standard groups all showed a substantial decrease in transfer latency compared to the DC group ($p < 0.05$, $p < 0.01$ and $p < 0.001$ respectively) (Table 13 and Figure 28).

The findings were examined with 6 rats within every group, and shown as the mean ± SEM. $^{\alpha}p < 0.001$, relative to the NC group; $^{a}p < 0.001$, $^{b}p < 0.01$, and $^{c}p < 0.05$, relative to DC group.

- *Effect of MEAP on the brain AChE levels*

Following the onset of Alzheimer's disease, the DC group had noticeably elevated AChE levels relative to the control group ($p < 0.001$). After applying MEAP 400 and standard, AChE levels dropped significantly ($p < 0.01$ and $p < 0.001$, correspondingly), in contrast to the control group. However, when comparing the NC group to MEAP 200, no significant difference was seen (Figure 29).

The findings were examined with 6 rats within every group, and shown as the mean±SEM. $^{\alpha}p < 0.001$, relative to the NC group; $^{a}p < 0.001$ and $^{b}p < 0.01$, relative to DC group.

DISCUSSION

Fresh *A. pungens* leaves were analysed by TLC, and it was concluded that the leaves contained a mixture of flavonoids. TLC analysis revealed that the flavonoid components quercetin and rutin, as well as the flavonoid glycoside stigmasterol, were concentrated in the methanol fraction, in comparison to the conventional compounds quercetin and rutin (fattysterol). Both quercetin and rutin were detected using HPTLC. Using nuclear magnetic resonance (NMR) analysis, the proton and carbon binding sites of the previously unknown compounds A and B were determined to be quercetin and rutin, respectively.

There is mounting evidence implicating a dysfunctional insulin signalling pathway in the etiology of AD, since both insulin and insulin receptor expression are reduced in the AD brain.[26,27] Diabetes mellitus and AD have both been linked to decreased insulin and insulin signalling transduction, according to many epidemiological and experimental investigations.[28,29] Streptozotocin (STZ) affects memory in rats via modifying the central nervous system (CNS) due to reduced cholinergic dysfunction, oxidative stress, chronic hyperglycemia, and abnormalities in the glucagon-like peptide. In the current investigation, mice were injected with STZ to create a diabetic mouse model. We discovered that STZ caused a dramatic rise in blood sugar after being administered. To determine whether hyperglycemia aggravated cerebral amyloidosis and behavioral impairments, and to investigate the underlying processes, we employed this model.

An animal model of T2DM was produced by treatment of streptozotocin (STZ) which generates a large increase in blood glucose by damaging β-cells. Prior studies have shown that streptozotocin is a strong toxin for these β-cells, and this toxin has been employed as an experimental model of hyperglycemia to identify anti-diabetic medicines.[30,31] BGL and OGTT findings from the current investigation supported the hypoglycemic potential of MEAP. The diabetes-induced group had higher BGLs than the control group, whereas the MEAP and conventional groups had lower glucose levels. In diabetic rats, MEAP exerts an effect similar to insulin, decreasing plasma glucose levels while increasing glucose absorption and decreasing hyperglycemia.

Prolonged hyperglycemia is the root cause of most diabetes complications, including cognitive deficits.[32] Antihyperglycemics and insulin sensitizers have been shown to improve diabetes patients' cognitive performance, according to studies.[33] In the present investigation, mice were given pharmacological therapy and then tested using the MWM & EPM to evaluate their memory and learning abilities. Mouse

escape latencies and TSTQ scores were lower in the diabetic group relative to the control group, but they were higher in the MEAP-treated group. The MEAP injection improved the transfer latency time day by day but in the case of diabetic mice, this change was very minimal. It was discovered that blocking muscarinic and cholinergic receptors may cause memory loss, but that MEAP can protect against this effect.

Significant inhibitory actions against alpha-amylase and alpha-glucosidase were seen after quercetin and rutin administration in the current investigation. Several prior research revealed that quercetin[34,35] and rutin[36,37] possess hypoglycemic effects *via* a number of different pathways. Therefore, quercetin and rutin's ability to lower hyperglycemia may account for the enhancement of cognitive acuity shown in diabetic rats.[38,39]

Learning, memory, and the cortical architecture of movement are all dependent on cholinergic neurotransmission.[40] The hydrolysis of acetylcholine by the enzyme acetylcholine esterase (AChE) has been shown to be a crucial step in ensuring proper cholinergic function.[41] It has been hypothesized that cholinesterases have a function in morphogenesis and neurodegenerative illnesses in addition to their involvement in cholinergic transmission.[42] Intriguingly, several studies have linked elevated AChE activity in the brains of diabetics to memory and thinking problems.[43,44] Also, quercetin,[45] rutin,[46] and the combination of the two[47] have all been found to be effective inhibitors of AChE. Inhibition of AChE by quercetin and rutin is therefore a key mechanism by which *A. pungens* protects against diabetes-related cognitive decline.

CONCLUSION

To sum up, therapy with *Alternanthera pungens* improved cognitive impairment in diabetic rats, suggesting that this herb may have therapeutic use in reversing neuronal deficiency in diabetes patients. The preventive benefits of *A. pungens* on metabolic dysfunction may be related to its various pleiotropic properties including antihyperglycemic and anticholinesterase activity. HPTLC may be useful in identifying and standardizing flavonoids in *A. pungens*, and the fingerprint analysis findings may be used as a reference for drug identification and quality control.

REFERENCES

1. Nguyen TT, Ta QT, Nguyen TK, Nguyen TT, Van Giau V. Type 3 diabetes and its role implications in Alzheimer's disease. International journal of molecular sciences. 2020 Apr 30;21(9):3165.
2. Watson GS, Craft S. The role of insulin resistance in the pathogenesis of Alzheimer's disease: implications for treatment. CNS drugs. 2003 Jan;17:27-45.
3. M de la Monte S. Brain insulin resistance and deficiency as therapeutic targets in Alzheimer's disease. Current Alzheimer Research. 2012 Jan 1;9(1):35-66.
4. Vinuesa A, Pomilio C, Gregosa A, Bentivegna M, Presa J, Bellotto M, Saravia F, Beauquis J. Inflammation and insulin resistance as risk factors and potential therapeutic targets for Alzheimer's disease. Frontiers in Neuroscience. 2021 Apr 23;15:653651.
5. Dineley KT, Jahrling JB, Denner L. Insulin resistance in Alzheimer's disease. Neurobiology of disease. 2014 Dec 1;72:92-103.
6. Farris W, Leissring MA, Hemming ML, Chang AY, Selkoe DJ. Alternative splicing of human insulin-degrading enzyme yields a novel isoform with a decreased ability to degrade insulin and amyloid β-protein. Biochemistry. 2005 May 3;44(17):6513-25.
7. Almermesh MH. *The Link Between Type 3 Diabetes and Alzheimer's Disease: Mechanisms of a Neuro-endocrine Disorder* (Doctoral dissertation, Massachusetts College of Pharmacy and Health Sciences).
8. Kilger E, Buehler A, Woelfing H, Kumar S, Kaeser SA, Nagarathinam A, Walter J, Jucker M, Coomaraswamy J. BRI2 Protein Regulates β-Amyloid Degradation by Increasing Levels of Secreted Insulin-degrading Enzyme (IDE). Journal of Biological Chemistry. 2011 Oct 28;286(43):37446-57.
9. Saavedra J, Nascimento M, Liz MA, Cardoso I. Key brain cell interactions and contributions to the pathogenesis of Alzheimer's disease. Frontiers in Cell and Developmental Biology. 2022 Nov 29;10:1036123.
10. Pokusa M, Kráľová Trančíková A. The central role of biometals maintains oxidative balance in the context of metabolic and neurodegenerative disorders. Oxidative Medicine and Cellular Longevity. 2017 Jul 2;2017.
11. Burillo J, Marqués P, Jiménez B, González-Blanco C, Benito M, Guillén C. Insulin resistance and diabetes mellitus in Alzheimer's disease. Cells. 2021 May 18;10(5):1236.
12. Kullmann S, Heni M, Hallschmid M, Fritsche A, Preissl H, Häring HU. Brain insulin resistance at the crossroads of metabolic and cognitive disorders in humans. Physiological reviews. 2016 Aug 3.
13. Kim B, Feldman EL. Insulin resistance as a key link for the increased risk of cognitive impairment in the metabolic syndrome. Experimental & molecular medicine. 2015 Mar;47(3):e149-.
14. Talbot K, Wang HY, Kazi H, Han LY, Bakshi KP, Stucky A, Fuino RL, Kawaguchi KR, Samoyedny AJ, Wilson RS, Arvanitakis Z. Demonstrated brain insulin resistance in Alzheimer's disease patients is associated with IGF-1 resistance, IRS-1 dysregulation, and cognitive decline. The Journal of clinical investigation. 2012 Apr 2;122(4):1316-38.
15. Ekblad L. Insulin resistance, cognition and brain amyloid accumulation. University of Turku. 2018.
16. Kandimalla R, Thirumala V, Reddy PH. Is Alzheimer's disease a type 3 diabetes? A critical appraisal. Biochimica and Biophysica Acta (BBA)-Molecular Basis of Disease. 2017 May 1;1863(5):1078-89.
17. Haas CB, Kalinine E, Zimmer ER, Hansel G, Brochier AW, Oses JP, Portela LV, Muller AP. Brain insulin administration triggers distinct cognitive and neurotrophic responses in young and aged rats. Molecular neurobiology. 2016 Nov;53:5807-17.
18. Tong M, Deochand C, Didsbury J, de la Monte SM. T3D-959: A multi-faceted disease remedial drug candidate for the treatment of Alzheimer's disease. Journal of Alzheimer's Disease. 2016 Jan 1;51(1):123-38.
19. Revathy S, Elumalai S, Antony MB. Isolation, purification and identification of curcuminoids from turmeric (Curcuma longa L.) by column chromatography. Journal of Experimental sciences. 2011 Jun 27;2(7).
20. Jaiswal S, Yadav DS, Mishra MK, Gupta AK. Detection of adulterants in spices through chemical method and thin layer chromatography for forensic consideration. Int J Dev Res. 2016 Jun 19;6(08):8824-7.
21. Xavier SK, Devkar RA, Chaudhary S, Shreedhara CS, Setty MM.

Pharmacognostical standardisation and HPTLC quantification of Gallic acid in Homonoia riparia Lour. Pharmacognosy Journal. 2015;7(6).
22. Kshirsagar RP, Kothamasu MV, Patil MA, Reddy GB, Kumar BD, Diwan PV. Geranium oil ameliorates endothelial dysfunction in high fat high sucrose diet induced metabolic complications in rats. Journal of Functional Foods. 2015 May 1;15:284-93.
23. Vorhees CV, Williams MT. Morris water maze: procedures for assessing spatial and related forms of learning and memory. Nature protocols. 2006 Aug;1(2):848-58.
24. Pentkowski NS, Berkowitz LE, Thompson SM, Drake EN, Olguin CR, Clark BJ. Anxiety-like behavior as an early endophenotype in the TgF344-AD rat model of Alzheimer's disease. Neurobiology of aging. 2018 Jan 1;61:169-76.
25. Khan RA, Khan MR, Sahreen S. Brain antioxidant markers, cognitive performance and acetylcholinesterase activity of rats: efficiency of Sonchus asper. Behavioral and Brain functions. 2012 Dec;8(1):1-7.
26. Griffith CM, Eid T, Rose GM, Patrylo PR. Evidence for altered insulin receptor signaling in Alzheimer's disease. Neuropharmacology. 2018 Jul 1;136:202-15.
27. Correia SC, Santos RX, Carvalho C, Cardoso S, Candeias E, Santos MS, Oliveira CR, Moreira PI. Insulin signaling, glucose metabolism and mitochondria: major players in Alzheimer's disease and diabetes interrelation. Brain research. 2012 Mar 2;1441:64-78.
28. De Felice FG, Ferreira ST. Inflammation, defective insulin signaling, and mitochondrial dysfunction as common molecular denominators connecting type 2 diabetes to Alzheimer disease. Diabetes. 2014 Jul 1;63(7):2262-72.
29. Akhtar A, Sah SP. Insulin signaling pathway and related molecules: role in neurodegeneration and Alzheimer's disease. Neurochemistry international. 2020 May 1;135:104707.
30. Rajappa R, Sireesh D, Salai MB, Ramkumar KM, Sarvajayakesavulu S, Madhunapantula SV. Treatment with naringenin elevates the activity of transcription factor Nrf2 to protect pancreatic β-cells from streptozotocin-induced diabetes in vitro and in vivo. Frontiers in Pharmacology. 2019 Jan 28;9:1562.
31. Zhang Y, Ren C, Lu G, Mu Z, Cui W, Gao H, Wang Y. Anti-diabetic effect of mulberry leaf polysaccharide by inhibiting pancreatic islet cell apoptosis and ameliorating insulin secretory capacity in diabetic rats. International immunopharmacology. 2014 Sep 1;22(1):248-57.
32. Saedi E, Gheini MR, Faiz F, Arami MA. Diabetes mellitus and cognitive impairments. World journal of diabetes. 2016 Sep 9;7(17):412.
33. Li XH, Xin X, Wang Y, Wu JZ, Jin ZD, Ma LN, Nie CJ, Xiao X, Hu Y, Jin MW. Pentamethylquercetin protects against diabetes-related cognitive deficits in diabetic Goto-Kakizaki rats. Journal of Alzheimer's Disease. 2013 Jan 1;34(3):755-67.
34. Alam MM, Meerza D, Naseem I. Protective effect of quercetin on hyperglycemia, oxidative stress and DNA damage in alloxan induced type 2 diabetic mice. Life sciences. 2014 Jul 25;109(1):8-14.
35. Oyedemi SO, Nwaogu G, Chukwuma CI, Adeyemi OT, Matsabisa MG, Swain SS, Aiyegoro OA. Quercetin modulates hyperglycemia by improving the pancreatic antioxidant status and enzymes activities linked with glucose metabolism in type 2 diabetes model of rats: In silico studies of molecular interaction of quercetin with hexokinase and catalase. Journal of food biochemistry. 2020 Feb;44(2):e13127.
36. Chen S, Li W, Jing S, Zheng W, Zhishu T. Hypoglycemic and hypolipidemic effects of rutin on hyperglycemic rats. Journal of Traditional Chinese Medicine. 2020 Aug 15;40(4):640.
37. Prince PS, Kamalakkannan N. Rutin improves glucose homeostasis in streptozotocin diabetic tissues by altering glycolytic and gluconeogenic enzymes. Journal of biochemical and molecular toxicology. 2006 Apr;20(2):96-102.
38. Xianchu L, Huan P, Kang L, Beiwang D, Ming L. Protective effect of rutin against diabetes-associated cognitive decline in rats. Pakistan Journal of Pharmaceutical Sciences. 2022 May 1;35(3).
39. Maciel RM, Carvalho FB, Olabiyi AA, Schmatz R, Gutierres JM, Stefanello N, Zanini D, Rosa MM, Andrade CM, Rubin MA, Schetinger MR. Neuroprotective effects of quercetin on memory and anxiogenic-like behavior in diabetic rats: Role of ectonucleotidases and acetylcholinesterase activities. Biomedicine & Pharmacotherapy. 2016 Dec 1;84:559-68.
40. Mesulam MM, Guillozet A, Shaw P, Levey A, Duysen EG, Lockridge O. Acetylcholinesterase knockouts establish central cholinergic pathways and can use butyrylcholinesterase to hydrolyze acetylcholine. neuroscience. 2002 Apr 3;110(4):627-39.
41. Lane RM, Potkin SG, Enz A. Targeting acetylcholinesterase and butyrylcholinesterase in dementia. International Journal of Neuropsychopharmacology. 2006 Feb 1;9(1):101-24.
42. Tiwari V, Kuhad A, Bishnoi M, Chopra K. Chronic treatment with tocotrienol, an isoform of vitamin E, prevents intracerebroventricular streptozotocin-induced cognitive impairment and oxidative–nitrosative stress in rats. Pharmacology Biochemistry and Behavior. 2009 Aug 1;93(2):183-9.
43. Rajput MS, Sarkar PD. Modulation of neuro-inflammatory condition, acetylcholinesterase and antioxidant levels by genistein attenuates diabetes associated cognitive decline in mice. Chemico-biological interactions. 2017 Apr 25;268:93-102.
44. Gaspar JM, Baptista FI, Macedo MP, Ambrosio AF. Inside the diabetic brain: role of different players involved in cognitive decline. ACS chemical neuroscience. 2016 Feb 17;7(2):131-42.
45. Adedara IA, Ego VC, Subair TI, Oyediran O, Farombi EO. Quercetin improves neurobehavioral performance through restoration of brain antioxidant status and acetylcholinesterase activity in manganese-treated rats. Neurochemical research. 2017 Apr;42:1219-29.
46. Yan X, Chen T, Zhang L, Du H. Study of the interactions of forsythiaside and rutin with acetylcholinesterase (AChE). International journal of biological macromolecules. 2018 Nov 1;119:1344-52.
47. Adefegha SA, Oboh G, Fakunle B, Oyeleye SI, Olasehinde TA. Quercetin, rutin, and their combinations modulate penile phosphodiesterase-5′, arginase, acetylcholinesterase, and angiotensin-I-converting enzyme activities: a comparative study. Comparative Clinical Pathology. 2018 May;27:773-80.